Preparation and Characterization of c-$LiMn_2O_4$ Thin Films prepared by Pulsed Laser Deposition for Lithium-Ion Batteries

Daniel Albrecht,* Hendrik Wulfmeier, and Holger Fritze[a]

In this work, lithium manganese oxide (LMO) thin films are prepared using pulsed laser deposition (PLD) at room temperature. The as-prepared films are amorphous and require a subsequent annealing step to achieve dense films of c-spinel LMO ($LiMn_2O_4$). We applied different annealing temperatures under an argon atmosphere to investigate the thermodynamics of the films and to find the minimum crystallization temperature. Thereby, a simple film deposition process with only one subsequent annealing step is developed to prepare crystalline films. The samples are characterized using scanning electron microscopy (SEM), secondary ion mass spectrometry (SIMS), X-ray diffraction (XRD), thin-film-calorimetry, impedance spectroscopy, and electrochemical methods. The results indicate that a narrow temperature range around 700 °C is suitable for the preparation of the spinel phase. Using this preparation route, no further crystalline phases could be identified by XRD. The electrochemical properties of the films are investigated and compared to electrodes made of commercially available LMO powders. The electrochemical characterization shows a capacity of 95 $mAh\,g^{-1}$ for the commercial powder and 110 $mAh\,g^{-1}$ for the thin-film samples.

Introduction

The thin-film preparation of active materials for lithium-ion-batteries (LIBs) is increasingly drawing attention in the scientific community for several reasons. Many physical characterization methods, including X-ray photoelectron spectroscopy (XPS), secondary ion mass spectrometry (SIMS), and Auger electron spectroscopy, require a smooth surface and compact structure to provide accurate results. Therefore, the results obtained using thin-film samples can be used for highly accurate and quantitative characterization. Smooth thin films can also be used as a reference material for investigations of the morphology's influence on the performance of active materials, as the size and shape of particles influence the electrochemical properties significantly. Another important factor for the increased focus on thin-film battery materials is their applicability in micro-LIBs. The micro-scaling of devices (e.g., sensors) is continuing to shrink the sizes of devices as well as their energy demand, which makes many stand-alone applications feasible, if micro-LIBs can be used for the power supply. These systems can be useful in a variety of fields, such as medical implants and devices, labs-on-chip, or micrometer-sized stand-alone sensor systems (e.g., microelectromechanical systems, MEMS).

Lithium manganese oxide (LMO) is a promising cathode material for LIBs because of its high theoretical capacity of 148 $mAh\,g^{-1}$.[1] Most of the commercially available systems use $LiCoO_2$ as cathode material, which contains more than 60 wt% of cobalt. As cobalt is known to be toxic and expensive, battery manufacturers are seeking a replacement for $LiCoO_2$ as cathode material.

The cubic spinel lithium manganese oxide ($LiMn_2O_4$, referred to as LMO) is a candidate material for the replacement of $LiCoO_2$ as manganese is cheaper than cobalt by more than a factor of 10 and less toxic.[2] Aside from the price, LMO shows several further advantages compared to $LiCoO_2$. The electrochemical potential against lithium is slightly higher than the potential of $LiCoO_2$ (4.1 V compared to 3.9 V).[1] Considering the safety of the assembled cells, $LiMn_2O_4$ also has a major advantage over $LiCoO_2$ in that the onset temperature of its oxygen release reaction is higher, and the thermal runaway reaction is less exothermic.[3]

In the literature, many examples of LMO thin-film preparations can be found. Electron-beam evaporation is used by Thackery;[4] Shui and his coworkers apply electrostatic spray deposition to prepare the layers.[5] Furthermore several sputtering techniques with and without the use of a reactive atmosphere are used for preparation.[6–8] Also some literature sources exist on the preparation of LMO thin films using pulsed laser deposition (PLD). Tang et al. applied elevated-temperature PLD to investigate the influence of the substrate temperature and the oxygen partial pressure on the film quality.[9] Morcrette et al.[10] investigated the effect of

[a] D. Albrecht, H. Wulfmeier, H. Fritze
Institute of Energy Research and Physical Technologies
Clausthal University of Technology
Am Stollen 19B, 38640 Goslar (Germany)
E-mail: Daniel.albrecht@tu-clausthal.de

Part of a Special Issue on "Li-Ion Batteries". To view the complete issue, visit: http://dx.doi.org/10.1002/ente.v4.12

stoichiometry deviations on the electrochemical properties, and Yamada and his coworkers focus on lithium-ion kinetics in LMO thin films.[11] To the best of our knowledge, the combination of LMO thin films prepared by room-temperature PLD deposition with subsequent annealing (along with the comparison to electrodes prepared with a commercial powder) has not been reported to this point. Provided that subsequent crystallization of the films is possible by annealing, the preparation using PLD at room temperature has an advantage in terms of cost-effective equipment and the number of process steps. Furthermore, a better understanding of the thermodynamics of the LMO thin films is gained, including the knowledge of the phase composition as function of the annealing temperature. In this work, the influence of the annealing process on the structure of the thin films is investigated. Samples showing the spinel structure are investigated by electrochemical methods and compared to a commercially available powder, which is also used for the preparation of the PLD targets.

Results and Discussion

Phase determination

For the general characterization of the thin films, Si substrates are used. Prior to the LMO deposition, a thin layer of alumina (Al_2O_3) is deposited onto the Si-Substrate to prevent the diffusion of Si into the active layer. The thin LMO film as well as the Al_2O_3 layer are deposited at room temperature and are therefore amorphous. To fabricate crystalline c-spinel $LiMn_2O_4$, which has a significantly higher capacity than other LMO polymorphs,[12] the samples require an annealing step. To investigate the behavior, five different temperatures ranging from 600 to 1000 °C are chosen. Annealing is performed in Ar-atmosphere to suppress further oxidation of the multi-layer components (e.g., formation of Li_2O), as the thin films are oxygen sensitive.

The annealing conditions are crucial to the film quality as was observed in the X-ray diffraction patterns in Figure 1, which indicates the onset of crystal growth at 600 °C. The sample annealed at 600 °C shows a small peak corresponding to the (044) plane reflections of c-$LiMn_2O_4$ at $2\theta \approx 64°$ whereas the (022) reflection is not visible due to the noise of the background signal. At an annealing temperature of 700 °C, clearly visible reflections appear corresponding to the (022), (113), (004), and (044) planes at diffraction angles of 30°, 36°, 44°, and 64°, respectively. Samples annealed at higher temperatures (900–1000 °C) show additional peaks not corresponding to the spinel-type LMO. At these higher temperatures the diffraction patterns indicate that at least one additional phase has evolved in addition to the c-spinel (marked with red arrows in Figure 1). The peak at $2\theta \approx 33°$ most likely indicates the formation of a tetragonal phase of LMO.[13] To ensure that all further investigations are made using a single-phase c-spinel sample, the samples annealed at 700 °C are chosen for further investigations.

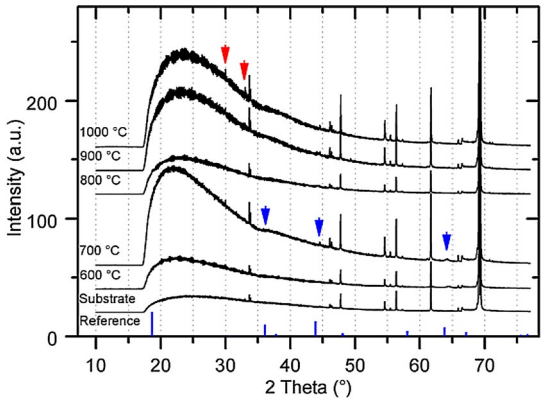

Figure 1. X-Ray diffraction patterns of samples annealed at 600–1000 °C and of the uncoated substrate. The reference refers to ICSD 89985. Reflections corresponding to cubic-$LiMn_2O_4$ are marked with blue arrows, and the red arrows mark reflections of LMO polymorphs that do not belong to c-$LiMn_2O_4$.

Figure 2 shows the morphology of the as-prepared and annealed samples. The as-prepared films do not contain major crystallites, which is the expected morphology following PLD deposition. We also observed that the film exhibits a very fine texture. In the SEM micrograph of the sample annealed at 600 °C, small uniformly distributed crystallites of approximately 100 nm in size are visible. Annealing of the samples at temperatures of 700, 800, and 900 °C results in further crystallite growth to average sizes of 200, 600, and 2000 nm, respectively. At an annealing temperature of 1000 °C the films convert to a closed agglomerated layer without visible pores. Further, the film starts to peel off from the substrate. The separation of the layer from the substrate as well as the

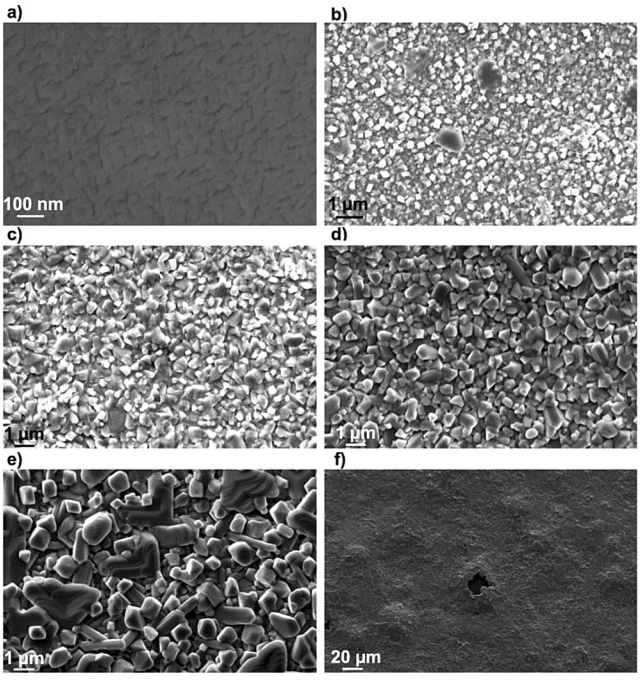

Figure 2. SEM of the prepared samples, annealed at different temperatures a) as prepared, b) 600 °C, c) 700 °C, d) 800 °C, e) 900 °C, f) 1000 °C.

complete structural change indicates the formation of a new phase, which is in good agreement with the XRD results.

Figure 3 shows the results from two thin-film calorimetric (TFC) measurements of LMO thin films investigated in Ar/H_2 (99.5 %/0.5 %) atmosphere (blue) and in ambient air (black). The measurement principle is based on highly temperature-sensitive planar temperature sensors consisting

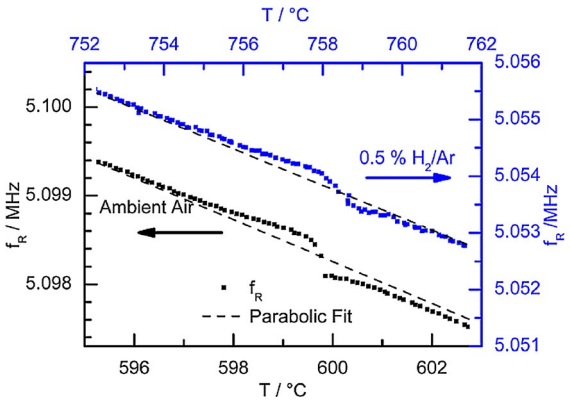

Figure 3. Thin film calorimetric measurement on LMO thin films in air and in 0.5 % H_2 in Ar. Plotted is the resonance frequency as a function of the furnace temperature.

of high-temperature stable langasite ($La_3Ga_5SiO_{14}$) resonators.[14] For calorimetric characterization, the material of interest is deposited on top of the resonator. As the resonance frequency (f_R) of the resonator is temperature dependent, a phase transition in the investigated film can be detected by a deviation of f_R from the undisturbed temperature dependence (dotted line). Figure 4 shows the resonance frequency

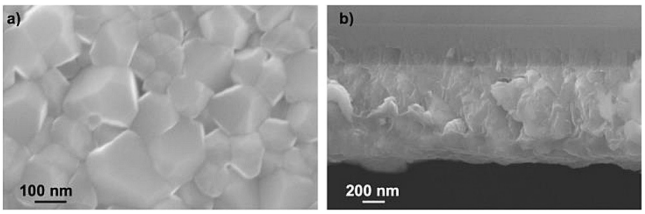

Figure 4. High-magnification SEM images of the sample annealed at 700 °C: a) top view b) cross section.

of the resonator over the temperature range of the furnace in the vicinity of the phase transition to c-$LiMn_2O_4$. For the sample annealed in Ar/H_2 atmosphere (low p_{O2}) the phase transition from a mixture of different phases (o-$LiMnO_2$ + *m*-$LiMnO_2$ + t-Mn_3O_4) to c-$LiMn_2O_4$ happens at a transition temperature of $T = 758$ °C. The black line shows another LMO thin-film sample investigated in air (high p_{O2}). In this system, the c-spinel phase is growing from the over-stoichiometric spinel phase $Li_{1.33}Mn_{1.67}O_4$ at a transition temperature of $T = 600$ °C. The reasons for these differences are still not fully understood. In publications focused on these phase transformations,[15,16] it is reported that the stoichiometric spinel phase crystallizes from different parent phases in different atmospheres, even though the starting composition is the same. The TFC results show that the phase mixture in the low-p_{O2} atmosphere has a higher thermal stability than the over-stoichiometric spinel, which is the parent phase in the atmosphere with higher oxygen partial pressure. A detailed introduction to the technique and detailed results of the LMO characterization are published elsewhere.[15,16] These results are in good agreement with the annealing behavior of the PLD-deposited LMO films presented here, where a single-phase sample is prepared at an annealing temperature of 700 °C, which is in between the two values from TFC characterization. As these results were obtained in a pure Ar-atmosphere (medium p_{O2}) the transition temperature is expected to be between 600 °C (high p_{O2}) and 785 °C (low p_{O2}), as confirmed by the XRD analysis.

As described above, samples annealed at 700 °C are chosen for further investigations. Figure 4 shows a high-magnification SEM micrograph. The cross-sectional SEM in Figure 4b reveals that a dense film of approximately 750 nm is grown, which has been confirmed by profilometric measurement (not shown here). In Figure 4b), the Al_2O_3 diffusion barrier is visible, whose thickness is measured by profilometry and found to be approximately 400 nm. It is noteworthy that the interface between the film and substrate is dense over the entire film, which indicates a good adhesion of the films to the substrate even though the LMO layer seems to inhibit some strain, as indicated in the XRD spectra.

Sample Composition

Figure 5 shows a depth profile determined by SIMS. In these experiments, the relative distributions of lithium, manganese, oxygen, silicon, and aluminum were recorded. It must be mentioned that the count-rate shown on the ordinate axis does not give absolute values for the concentration, as several effects, including elemental sensitivity and choice of isotopes, have to be considered. Nevertheless, the measurement shown here provides useful information about the elemental

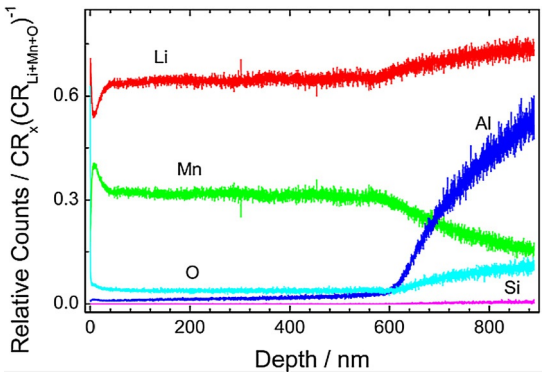

Figure 5. SIMS depth profile of the sample annealed at 700 °C measured in Cs cluster mode. Plotted are the count ratios of the shown elements divided by the sum of the Li, Mn, and O signals.

distribution as a function of depth in this multi-layer system. One can notice that the relative ratio of lithium, manganese, and oxygen is constant all the way towards the alumina diffusion barrier, thereby indicating a constant stoichiometry through the depth of the film. In previous investigations, Si diffusion into LMO (and thereby contamination of the active layer) has been a major issue during sample processing. It is noteworthy that the barrier layer effectively prevents Si diffusion into the LMO layer. During annealing, silicon diffuses into the Al_2O_3 layer to some extent, as was observed by the simultaneous increase of the Si and Al signals. However, the Si-signal is negligible throughout the LMO layer, which qualifies Al_2O_3 as an effective diffusion barrier.

Electrochemical Characterization

Electrochemical characterization is performed using lithium half-cells. For the electrochemical measurements, stainless-steel substrates are used to ensure good electrical contact. Figure 6a shows the data from cyclic voltammetry (CV) of a thin-film sample annealed at 700 °C, and Figure 6b shows a commercially available powder compacted with binder and conductive carbon to form an electrode. In case of the thin-film sample, a LMO film is deposited on stainless steel without further additives.

The CV curves of both LMO samples show the characteristic two-step lithiation reaction in the current response. This behavior of LMO is well described in the literature. Julien et al. experimentally proved that Li ions are (de-)intercalated in different tetrahedral sites.[17,18] In their work, the intercalation processes for the different sites are found to occur at slightly different potentials with a $\Delta U \approx 100$ mV by using galvanostatic cycling with potential limits (GCPL). This corresponds well to our work as presented in Figure 7. In our CV

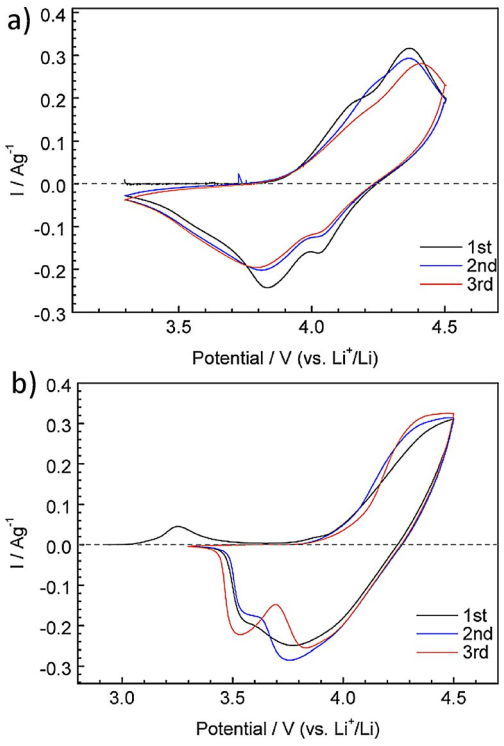

Figure 6. Cyclic voltammogram of the first three cycles of the 700 °C thin-film sample (a) and the commercial reference sample (b). Measurements are performed in a Li–LMO half-cell (as described in the Experimental-section) in a potential window of 3.3–4.5 V.

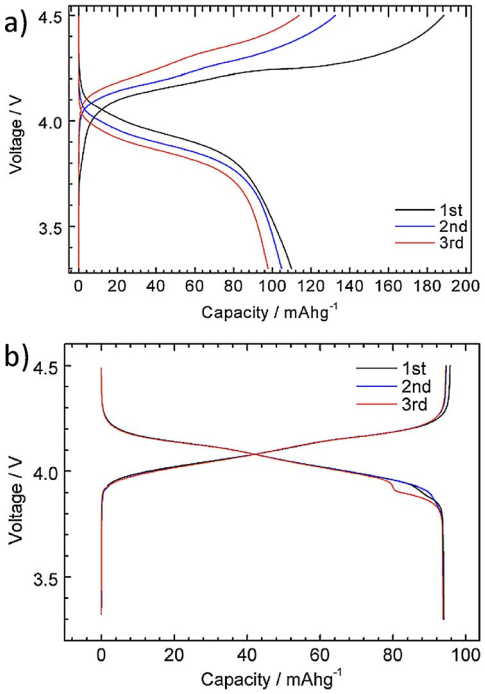

Figure 7. GCPL characterization of a thin-film sample (a) in comparison to a commercial powder electrode (b). The electrodes were cycled between 3.3 and 4.5 V in Li–LMO half-cell setups.

data of the thin-film sample, the deintercalation peak doublet at half-cell potentials of 4.17 and 4.37 V are clearly visible during the first cycle, but the potential differences of the current maxima are slightly higher ($\Delta U \approx 200$ mV), which is due to the different measurement techniques. In subsequent cycles, the deintercalation peak at 4.17 V decreases and is barely visible in the third cycle. Detailed interpretation of the third cycle data is not recommended as the thin-film sample is investigated using an open-cell setup, but inside a glove box. The open test cell allows the volatile electrolyte components (such as the diethyl carbonate) to evaporate, thereby influencing the performance of the cell as a whole. Experiments using a closed-cell setup are described below.

Tang et al. investigated LMO thin films deposited at different substrate temperatures.[9] Their results reveal an electrical potential difference of $\Delta U \approx 150$ mV, which is very close to the value shown here. The maximum of the current response during the intercalation of the thin film is presented in Figure 6a at half-cell potentials of 4.03 and 3.84 V.

Upon further analysis, several differences between the thin-film and the powder samples become clear. Though the different (de-)intercalation peaks of the thin-film sample can be clearly separated, the powder sample shows no clear cur-

rent peak separation in the CV data. The reason for this difference is most likely the higher degree of crystallinity in the thin-film sample, which results in a higher degree of order inside the host lattice and accordingly a more defined current response in CV. Another difference between the electrochemical behaviors of the samples is the voltage dependence of the redox couples during CV. The thin-film sample redox couples are at 3.84/4.17 V and 4.03/4.37 V, respectively, whereas the redox couples in the powder reference can be hardly distinguished.

Another major difference between both types of LMO electrodes becomes clear during lithiation. Bruce et al. report that nanostructured LMO shows a reversible phase transition between the cubic and tetragonal phase during deep lithiation induced by Jahn–Teller distortion.[19] This phase transition has a thermodynamic potential of approximately 2.96 V, but because of non-equilibrium conditions during cycling this effect is also observed at higher half-cell potentials. In this work, the influence of Jahn–Teller distortion is observed in the low potential region (≈3.55 V) of the CV lithiation slope for the powder sample as well as in GCPL in the form of an additional plateau at approximately 3.85 V. For the thin-film sample, this effect is not visible even though the potential window is identical for both samples, thereby indicating a homogeneous lithiation of the thin-film samples and thus improved electrode stability.

Further differences between the thin-film and powder samples are observed in the GCPL data shown in Figure 7. The initial charge capacity of the thin-film

sample is approximately 100 mAh g^{-1} higher than for the powder sample, whereas the first-cycle discharge capacity is only 20 mAh g^{-1} higher, indicating a poor cycling efficiency during the first cycle. Generally, the electrochemical capacity of the thin film is slightly higher during the three cycles performed.

Also notable is the fact that in all investigated GCPL measurements, the two-plateau behavior of LMO is visible, consisting of an S-shaped low potential plateau, which indicates a one-phase (de-)lithiation reaction and a second constant plateau at slightly higher potentials, which is indicative of a two-phase reaction. According to literature data,[17,18] the second phase in the low potential plateau is a λ-MnO_2 phase, which also has the spinel structure but a slightly lower lattice constant, thereby leading to different energies for the (de-)intercalation of lithium ions.

As mentioned above, a deep analysis of capacity retention on the thin-film sample shown in Figure 7 is not meaningful, as the measurement was performed using an open cell. Therefore the thin-film samples were also cycled in coin cells. Figure 8 shows the cycling stability of the thin-film electrode cycled with a C-rate of *C*/2. The cycling stability of these electrodes at such a high *C*-rate is poor. The capacity decreases from 70 mAh g^{-1} during the initial cycle to less than 20 mAh g^{-1} in cycle 24, which is considerably less stable than other $LiMn_2O_4$ thin films investigated in literature.[8,9]

The cell used for the cycling experiment as presented in Figure 8 is also investigated using impedance spectroscopy

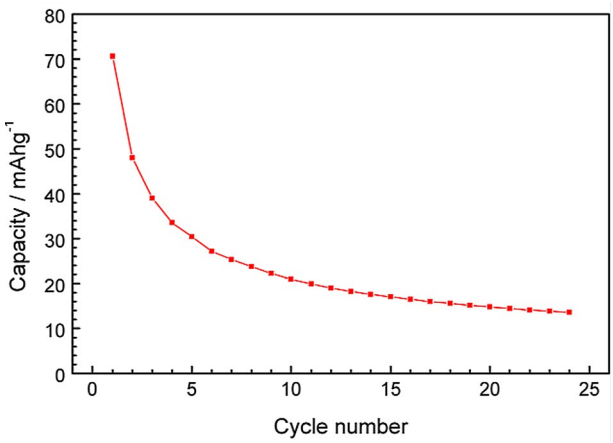

Figure 8. Investigation of the capacity fade of the thin-film electrode over the first 24 cycles at a *C*-rate of *C*/2.

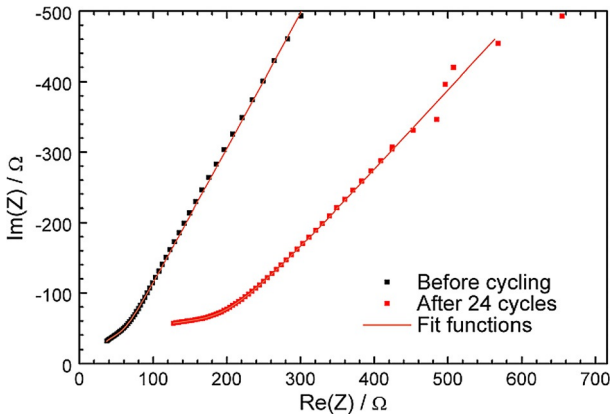

Figure 9. Impedance spectra (1 Hz–20 kHz) of a thin-film cell before cycling (blue) and after 24 cycles (red). The orange line represents the fit function from the equivalent circuit.

before and after cycling. The obtained impedance spectra, shown in Figure 9, are fitted using an equivalent circuit consisting of a parallel arrangement of a constant-phase element and a resistor in series with a Warburg element (open). The resistance changes from 22 Ω before cycling to 132 Ω after 24 cycles, which indicates an increase in internal cell resistance by a factor of approximately 6. The specific conductivity of the $LiMn_2O_4$ is also measured using impedance spectroscopy. The measured value of 5.8×10^{-5} S cm^{-1} is in good agreement with the values presented in Ref. [20].

Conclusions

In this work we present a simple approach for the preparation of c-spinel-LMO thin films. High-quality thin films can be prepared using room-temperature pulsed laser deposition with a subsequent annealing step. Single-phase c-$LiMn_2O_4$ samples are prepared using an annealing temperature of 700 °C. The electrochemical properties of the obtained samples are investigated using lithium half-cells. All measure-

ments show the distinct two-plateau behavior during (de-)lithiation. GCPL tests reveal a reversible capacity of 100 $mAhg^{-1}$ for the thin films, which is slightly higher than the capacity of the electrodes prepared using commercially available powders and thereby indicates an enhanced lithiation behavior of the thin films.

Experimental Section

Thin-film deposition: Preparation of LMO thin films was performed using a pulsed laser deposition system with a KrF excimer laser (Compex Pro 205, Lambda Physics); the wavelength was 248 nm and the typical pulse length was 25 ns. Pieces of Si (100) wafer with 10×10 mm^2 were used as substrates for general characterization. Before LMO deposition, a thin Al_2O_3 film was deposited onto the substrates to prevent interlayer diffusion during annealing of the LMO films. For Al_2O_3 deposition, a sintered alumina target (Friatec) was used. The laser pulse characteristics chosen were pulse energies of 250 mJ with a repetition rate of 15 Hz, and the deposition was performed for 10 min. The total pressure in the UHV chamber was 2×10^{-3} Pa without additional reactive gas flow. Deposition of the LMO layers was performed using a pulse energy of 200 mJ and a repetition rate of 15 Hz over a period of 60 min. For a spot size of 2 mm^2 the laser fluence was calculated to be 10 $J\,cm^{-2}$. The target was prepared using a commercial $LiMn_2O_4$ powder pressed to pellets at a pressure of $p\approx520$ MPa at room temperature. After deposition of the Al_2O_3 and LMO films, the samples were annealed in a tube furnace at temperatures ranging from 600 to 1000 °C under an Ar atmosphere (purity 99.996 %). As the electrical contact was crucial, thin-film samples for electrochemical characterization were deposited onto stainless-steel substrates using the same parameters, but without the Al_2O_3 layer. The reference samples were prepared from commercial powder. The coating of the Al current collector was performed using the doctor blade technique. The slurry was prepared with a weight ratio of 90 % active material, 6 % C65, and 4 % polyvinylidene fluoride (PVDF) binder.

Phase characterization: X-ray diffraction was performed using $Cu_{K\alpha}$ radiation and a Bragg Brentano geometry diffractometer (D5005, Siemens) with sample rotation. The micrographs were recorded using an SEM (MA 10, Carl Zeiss and a Super Ultra Series Column; Carl Zeiss for the high-resolution images). For depth profiling of the multilayer systems, a SIMS/secondary neutral mass spectrometry (SNMS) system (SIMS/SNMS Workstation, Hiden Analytical) with a Cs^+-ion source was used. To prevent faulty signals, the profiles were recorded in Cs cluster mode, scanning for atomic masses 140, 188, 149, 160, and 161 for Li, Mn, O, Al, and Si, respectively.

Thin-film calorimetry: Calorimetric measurements on the samples were performed using the temperature dependence of the resonance frequency of langasite ($La_3Ga_5SiO_{14}$) resonators, which is a high-temperature stable piezoelectric material. The resonators were coated with keyhole-shaped platinum electrodes on both sides. Afterwards the material of interest was deposited on top of the electrodes. For the data shown in this work, a sputter process was used to deposit LMO on top of the resonators. Determination of the resonance frequency was performed using a high-speed network analyzer (E5100A, Agilent). The setup (including sample) could be inserted to a vertical tube furnace with a maximum temperature of 1100 °C (Linn High Therm). Temperature measurement was performed using a type S thermocouple in the direct vicinity of the sample.

Electrochemical characterization: Electrochemical measurements of the thin-film samples were performed in lithium half-cells with an open PTFE cell setup. For the characterization of the commercial powders closed laboratory cells (ECC-Combi, EL-Cell) were used. As electrolyte, 1 M $LiPF_6$ in ethylene carbonate:-diethyl carbonate (EC:DEC) was used for both cell types. CVs and GCPL measurements were performed using a Solartron 1287 for the thin-film samples and a BioLogic VSP240 apparatus for the commercial powder cells. CV measurements were performed at a scan speed of 0.5 $mV\,s^{-1}$. Cell preparation and thin-film characterization were performed in an Ar-filled glove box with O_2 and H_2O levels below 1 ppm. Cycling stability was tested with 2032 type coin cells and a BioLogic MPG-2 potentiostat, which was also used for electrochemical impedance spectroscopy (EIS). For the EIS measurements a frequency range from 1 Hz to 20 kHz with an amplitude of 20 mV was used.

Electrical characterization: For the determination of the specific conductivity of the layer, impedance spectroscopy from 1 Hz to 1 MHz with an amplitude of 1 V was performed. For these measurements, a Solartron 1260 was used. The impedance was measured between two gold electrodes on top of the layer.

Acknowledgements

The authors thank the Energie-Forschungszentrum Niedersachsen and the Ministry of Science and Culture for funding in the frame of the GEENI Graduate Program for Energy Storage and Electromobility. A special thanks goes to A. Oberland, S. Wagner, and M. Lepple for providing measurement capacities for the electrochemical characterization of the reference powders. We thank W. Dziony for his help with the SEMs as well as M. Schulz and R. Feder for supporting the SIMS measurements.

Keywords: electrochemistry · energy storage · lithium-ion batteries · lithium manganese oxide · pulsed laser deposition

[1] M. Sterner, I. Stadler in *Energiespeicher*, Springer, Berlin, **2014**, pp. 252.
[2] Data from "London Metal Exchange" www.lme.com January 2016.
[3] D. Doughty, E. P. Roth, *Electrochem. Soc. Interface* **2012**, *2*, 37–44.
[4] M. M. Thackeray, *J. Electrochem. Soc.* **1997**, *144*, L100–102.
[5] J. L. Shui, G. S. Jiang, S. Xie, C. H. Chen, *Electrochim. Acta* **2004**, *49*, 2209–2213.
[6] T. Brousse, P. Fragnaud, R. Marchand, D. M. Schleich, O. Bohnke, K. West, *J. Power Sources* **1997**, *68*, 412–415.
[7] K. F. Chiu, H. C. Lin, K. M. Lin, C. H. Tsai, *J. Electrochem. Soc.* **2005**, *152*, A2058–A2062.
[8] J. Fischer, C. Adelheim, T. Bergfeldt, K. Chang, C. Ziebert, H. Leiste, M. Stüber, S. Ulrich, D. Music, B. Hallstedt, H. J. Seifert, *Thin Solid Films* **2013**, *528*, 217–223.
[9] S. B. Tang, M. O. Lai, L. Lu, S. Tripathy, *J. Solid State Chem.* **2006**, *179*, 3831–3838.
[10] M. Morcrette, P. Barboux, J. Perriére, T. Brousse, A. Traverse, J. P. Boilot, *Solid State Ionics* **2001**, *138*, 213–219.
[11] I. Yamada, T. Abe, Y. Iriyama, Z. Ogumi, *Electrochem. Commun.* **2003**, *5*, 502–505.
[12] N. Kuwata, R. Kumar, K. Toribani, T. Suzuki, T. Hattori, J. Kawamura, *Solid State Ionics* **2006**, *177*, 2827–2832.

[13] M. M. Thackeray, P. J. Johnson, L. A. de Picciotto, P. G. Bruce, J. B. Goodenough, *Mater. Res. Bull.* **1984**, *19*, 179–187.
[14] H. Seh, H. L. Tuller, H. Fritze, *J. Eur. Ceram. Soc.* **2004**, *24*, 1425–1429.
[15] H. Wulfmeier, D. Albrecht, J. Fischer, S. Ivanov, A. Bund, S. Ulrich, H. Fritze, *J. Electrochem. Soc.* **2015**, *162*, A727–A736.
[16] H. Wulfmeier, D. Albrecht, J. Fischer, S. Ivanov, A. Bund, S. Ulrich, H. Fritze, *J. Mater. Sci.* **2013**, *48*, 6585–6596.
[17] C. Julien, *Ionics* **2000**, *6*, 30–45.
[18] C. M. Julien, *Mater. Sci. Eng.* **2003**, *40*, 47–102.
[19] P. G. Bruce, B. Scrosati, J. M. Tarascon, *Angew. Chem. Int. Ed.* **2008**, *47*, 2930–2946; *Angew. Chem.* **2008**, *120*, 2972–2989.
[20] J. Marzec, K. Swierak, J. Przewoznik, J. Molenda, D. R. Simon, E. M. Kelder, J. Schoonman, *Solid State Ionics* **2002**, *146*, 225–237.

Received: February 26, 2016
Published online on July 27, 2016

